MODELING AND SIMULATION OF WIND ENERGY CONVERSION SYSTEM USING PWM CONVERTERS

by

Tolga SÜRGEVİL

January, 2004

İZMİR

ABSTRACT

In this thesis, a DSP based pulse-width-modulated dual voltage source converter double-cage induction machine drive for wind energy conversion system is presented. The modeling of the double-cage induction machine is obtained. The determination of the equivalent circuit parameters of the induction machine is achieved by applying genetic algorithm. The converters are designed and implemented with a single fixed-point DSP to control the power flow in a wind energy conversion system. In the implementation, two digital PI controllers are used in dc link voltage regulation and rotor speed control. The methods rely on hysteresis current control and slip regulation technique on the line-side and machine-side converter, respectively. The results obtained from computer simulations of the complete mathematical model of the system are compared to experimental work carried in laboratory. Finally, the implemented system is tested with a 5kW wind turbine in the campus.

ÖZET

Bu tezde DSP tabanlı darbe genişlik bindirimi tekniğini kullanan çeviricilerin çift-kafes asenkron makina sürücüsü olarak rüzgar enerjisi dönüşümü sisteminde uygulanması amaçlanmıştır. Çift kafesli asenkron makinanın matematiksel modellemeleri yapılmıştır. Asenkron makinanın eşdeğer devre parametreleri genetik algoritma yöntemi uygulanarak bulunmuştur. Rüzgar enerjisi dönüşüm sisteminde güç akışını denetlemek amacıyla çeviriciler tek bir sayısal işaret işlemci kullanılarak tasarlanmış ve uygulanmıştır. Uygulamada dc link gerilimini ve mil hızını denetlemek için iki sayısal PI denetleyici tasarlanmıştır. Şebeke ve jeneratör tarafı çeviricilerde sırasıyla histeresis akım denetimi ve kayma faktörü regülasyonu yöntemlerinden yararlanılmıştır. Sistemin matematiksel modelleri kullanılarak elde edilen bilgisayar benzetimleri sonuçları laboratuvarda uygulanan sistemden elde edilen deneysel sonuçlarla karşılaştırılmıştır. Son olarak gerçekleştirilen sistem kampüs içerisinde kurulan 5kW gücünde rüzgar türbini ile test edilmiştir.

1. Introduction

The use of wind power has been in existence for over 3000 years, especially in mechanical systems for water pumping and grain grinding. The utilization of wind power for electricity generation is not a new concept and this idea was first realized in 1891. Since then, step by step improvements were made in this technology, but it is not considered to be the consistent source for providing electric power. In 1970s, the researches on the wind power systems are encouraged by the oil price shock and the improvements of power electronics applications on power control. The fact of that fossil fuel resources are not renewable and have harmful impacts on environment prompted the researches to focus on clean and safe energy resources as an alternative. During last decades, an increasing interest has emerged on wind energy technology and it is considered to be one of the most important renewable energy resources (Hansen et al, 2001), (Ackermann & Söder, 2000), (Walker & Jenkins 1997). Today, it is one of the rapidly growing technologies and markets. By the end of 2003, the total installed capacity of wind energy is estimated to be more than 35,000 MW all around the world (WEB_1).

Due to the advances in power electronics technology, the use of power electronic converters in wind energy conversion systems has rapidly been growing. With the improved reliability, higher power ratings, and lower price per kilowatts of the power electronic components, the techniques used in torque and speed control of synchronous and induction machines are mostly applied in wind energy conversion systems. The main advantages of employing power electronic converters are that they allow the variable-speed operation in order to maximize the power production of the wind turbine and enhanced control (Zinger & Muljadi, 1997), (Hansen et al, 2001). A well known fact is that a good matching of the coupled energy conversion devices (i.e. wind turbine and generator) is essential since the conversion efficiency is determined through the interaction of these devices (Buehring & Freris, 1981). Power electronic converters provide and interface between the generator terminals and the utility grid line or autonomous loads. Hence, various control techniques that employ different power electronic converter topologies are proposed depending on

the system and generator types as well as the required conversion and control purpose (Khater, 1996).

Many different power electronic converters are used in wind energy conversion systems. These are used for converting power from one ac system to another; typically, from the constant voltage constant frequency ac grid line to variable voltage variable frequency generator in such systems. There are many circuit topologies for ac to ac power conversion. In such converters, two common approaches can be used. These are direct conversion, such as in cycloconverters or matrix converters (Skvarenina, 2002) and dc link conversion, also called ac-dc-ac conversion (Kassakian et al, 1991). Two back to back there-phase voltage source converters (VSCs) using pulse width modulation (PWM) technique fall under the second category. An intermediate dc link is provided between two converters via a capacitor. This intermediate stage provides energy storage and filtering function. Since the converters on the line-side and machine-side are decoupled by a dc link capacitor, the two converters can be controlled separately (Hansen et al, 2001). These active converters can provide bidirectional power flow between two ac systems. The use of back to back PWM VSCs in wind energy applications is widespread because of this bidirectional power flow ability and various control strategies have been proposed (Simoes et al, 1997), (Pena et al, 2001). Moreover, due to the advantages of adjustable power factor and low total harmonic distortion of the ac mains currents of the back to back PWM converters, this circuit topology is considered to be an ideal frequency changer and solution to the problems of conventional diode or thyristor based drives (Singh et al, 1999). Due to the standards limiting the harmonic pollution of electrical mains, it becomes necessary to modify power electronic equipments interfacing to power supply lines. Hence, PWM converters are being considered to be the prime candidates as a reliable power electronic interface in applications that require bidirectional power flow (Liserre, 2001). This converter topology provides sinusoidal ac line currents at a desired power factor at the ac grid or line-side. Hence, this feature of adjustable power factor in these converters also allows their use as active filters for minimizing current harmonics of the polluting loads in ac power systems or VAR compensation (Akagi et al, 1990).

The purpose of this thesis is to design the DSP based PWM voltage source converters (VSCs) feeding a double-cage induction machine (DCIM) in a grid-connected wind energy conversion system. The modeling and implementation of the proposed system will be given in this thesis. The block scheme of the proposed system is given in Figure 1. The system consists of two back to back PWM VSCs, which provides a power electronic interface between the DCIM terminals and the utility grid line. The wind turbine is a propeller type, three-bladed turbine and coupled to the DCIM shaft through a gearbox. The generator is a 3-phase 4-pole induction machine with double-cage rotor. Since the starting torque of the wind turbine is low, the DCIM should satisfy the torque required for the startup of the system. The system can be started by driving the DCIM as motor via PWM converters, which allow both generator and motor operation of the DCIM. The PWM VSC at the line-side is connected to the ac grid through series inductors. These series inductors on each phase of the ac line are required for line current harmonic filtering and boost operation of the PWM VSC at the line-side. The control of both line current and dc link voltage can be achieved in these converters. The ac currents of the line-side converter and dc link voltage are controlled by hysteresis current control (HCC). The speed control of the DCIM is achieved by employing the slip regulation technique because it provides inherent current limiting and reduces the amount of measurement devices. The complete control of the system is carried out by the software developed on the TMS320F240 DSP, which is a fixed-point processor of Texas Instruments C24X family. Required computations and generation of switching signals based on the proposed control logic are performed on DSP. In closed-loop control schemes, the digital proportional-integral (PI) and fuzzy logic control (FLC) approaches are implemented. A detailed analysis and mathematical modeling of the parts in the drive system are obtained. The implementation of the drive system was tested in the laboratory and employed in the wind turbine built in the university campus. The results obtained from computer simulations and experiments are compared.

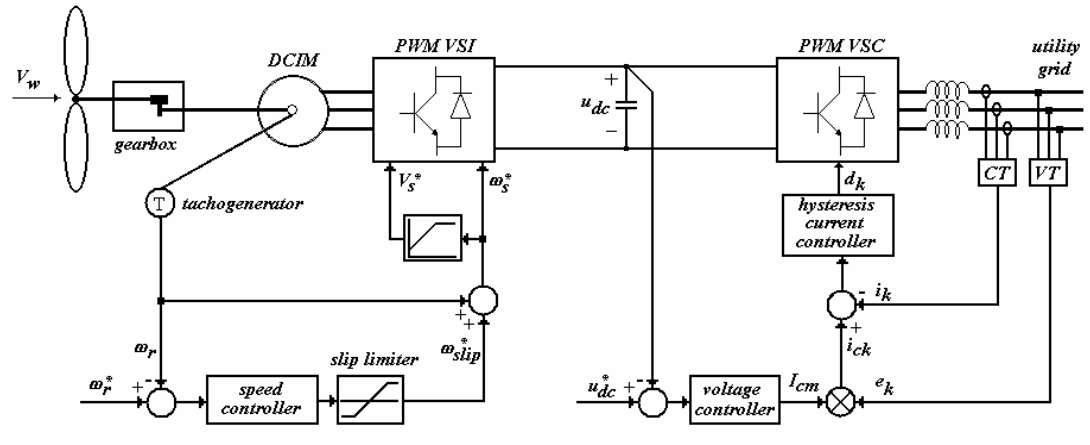

Figure 1. Variable speed wind generation system

2. Modeling of the Double-Cage Induction Machine

In the modeling of the DCIM, three more equations are needed in addition to single-cage machine model in order to represent the second rotor circuit in terms of machine variables. The dq/dq model of a double-cage induction motor includes the mutual inductance between top and bottom rotor slots (Adkins & Harley, 1975). Also, the reduced order models have been obtained from the qd/qd model of the machine deduced from the universal machine model (Khalil et al, 1982), (Richards, 1988), (Richards & Sarma, 1994). But, the inductance L_{23} does not exist in these models, since the field and damper windings of a synchronous machine are being interpreted as the upper and bottom cages for the DCIM. In this section, the derivation of the abc/qd model of the double-cage induction machine will be introduced. The motor parameters in the exact equivalent circuit are estimated from the genetic algorithm, and used for transient and steady state analysis of the machine. The results of digital simulation using dynamic models are compared to the experimental results.

2.1 Voltage Equations in abc/qd Reference Frame

The voltage equations expressed in terms of machine variables contain time-varying inductances and this introduces difficulty in the analysis of the machine. In order to eliminate these time-varying inductances and to obtain the abc/qd model of

the machine, transformations are applied to rotor variables of the machine. Hence, the time-varying inductances of the machine are transformed into time-invariant form as described in reference-frame theory (Krause et al, 1994). The rotor variables, which are expressed in machine variables and denoted by abc, are transformed into qd0 variables by applying the following transformation matrix

$$\mathbf{K_r} = \frac{2}{3}\begin{bmatrix} \cos\beta & \cos(\beta-120^o) & \cos(\beta+120^o) \\ \sin\beta & \sin(\beta-120^o) & \sin(\beta+120^o) \\ \frac{1}{2} & \frac{1}{2} & \frac{1}{2} \end{bmatrix} \tag{1}$$

where $\beta = \theta - \theta_r$ and

$$\theta = \int_0^t \omega(\xi)d\xi + \theta(0) \tag{2}$$

and ξ is dummy integration variable. $\omega(\xi)$ defines the angular speed of the reference frame and θ_r is angular displacement of the rotor. Applying this transformation to rotor abc variables, the voltage equations are expressed in stationary reference frame by letting $\omega = 0$ and rearranged in compact form with zero sequence equations are omitted as follows (Sürgevil & Akpınar, 2003)

$$\begin{bmatrix} v_{a1} \\ v_{b1} \\ v_{c1} \\ v'_{q2} \\ v'_{d2} \\ v'_{q3} \\ v'_{d3} \end{bmatrix} = \begin{bmatrix} r_1+L_{11}p & 0 & 0 & Mp & 0 & Mp & 0 \\ 0 & r_1+L_{11}p & 0 & -\frac{1}{2}Mp & -\frac{\sqrt{3}}{2}Mp & -\frac{1}{2}Mp & -\frac{\sqrt{3}}{2}Mp \\ 0 & 0 & r_1+L_{11}p & -\frac{1}{2}Mp & \frac{\sqrt{3}}{2}Mp & -\frac{1}{2}Mp & \frac{\sqrt{3}}{2}Mp \\ Mp & \omega_r\frac{\sqrt{3}}{2}L_m & -\omega_r\frac{\sqrt{3}}{2}L_m & r'_2+(L'_{22}+L'_{23})p & -\omega_r(L'_{22}+L'_{23}) & (L'_{23}+M)p & -\omega_r(M+L'_{23}) \\ \omega_r M & -\frac{\sqrt{3}}{2}L_m p & \frac{\sqrt{3}}{2}L_m p & \omega_r(L'_{22}+L'_{23}) & r'_2+(L'_{22}+L'_{23})p & \omega_r(M+L'_{23}) & (L'_{23}+M)p \\ Mp & \omega_r\frac{\sqrt{3}}{2}L_m & -\omega_r\frac{\sqrt{3}}{2}L_m & (L'_{23}+M)p & -\omega_r(M+L'_{23}) & r'_3+(L'_{33}+L'_{23})p & -\omega_r(L'_{33}+L'_{23}) \\ \omega_r M & -\frac{\sqrt{3}}{2}L_m p & \frac{\sqrt{3}}{2}L_m p & \omega_r(M+L'_{23}) & (L'_{23}+M)p & \omega_r(L'_{33}+L'_{23}) & r'_3+(L'_{33}+L'_{23})p \end{bmatrix} \begin{bmatrix} i_{a1} \\ i_{b1} \\ i_{c1} \\ i'_{q2} \\ i'_{d2} \\ i'_{q3} \\ i'_{d3} \end{bmatrix} \tag{3}$$

2.2 Torque Expression

The relation between the torque and rotor speed for the induction machine is given by the equation as follows

$$T_e = J\left(\frac{2}{P}\right)p\omega_r + T_L \tag{4}$$

Here, J is the inertia of the rotor, ω_r is the electrical rotor speed, P is the number of poles, T_L is the load torque on the shaft of the machine, and T_e is electromagnetic torque developed by the double-cage induction machine. In order to express the electromagnetic torque in terms of abc/qd variables, transformations given in equations (1) is applied to the rotor variables. The electromagnetic torque is expressed in terms of abc/qd variables as

$$T_e = \left(\frac{P}{2}\right)M\left\{\begin{array}{l} i'_{d2}(i_{a1} - \frac{1}{2}i_{b1} - \frac{1}{2}i_{c1}) + \frac{\sqrt{3}}{2}i'_{q2}(i_{b2} - i_{c2}) \\ + i'_{d3}(i_{a1} - \frac{1}{2}i_{b1} - \frac{1}{2}i_{c1}) + \frac{\sqrt{3}}{2}i'_{q3}(i_{b2} - i_{c2}) \end{array}\right\} \tag{5}$$

2.3 Determination of Machine Parameters using Genetic Algorithm

The equivalent circuit of the DCIM is given in Figure 2. The parameter determination of a double-cage induction machine is quite a difficult task with respect to a single-cage machine. Because the additional rotor windings make the analysis of the equivalent circuit more complicated. Hence, optimization techniques are applied in the determination of the machine parameters.

The Genetic Algorithm (GA) is an evolution program, which uses an iterative procedure to measure of its fitness function from the generated population of potential solutions. The members of the generated population are expressed in binary digits (or chromosomes) and the strength of each member is measured using the

fitness function. At each iterative step, a new population is generated, by altering some members of the population using genetic operators, crossover and mutation, to fit more individuals to the solution. The generation of new populations continues until the best population is obtained to fit an optimum solution. The GA is applied to problems to find a global maximum/minimum of multivariable equations. The main advantage of GA is that it provides global optimum of the cost (fitness) function without good estimation of initial values of the variables and the derivatives of the cost and constraints. During the application of the GA to an optimization problem, 6 stages given below should be completed: a) determination of the problem, b) genetic representation, c) creation of initial population, d) an evaluation function, e) genetic operators, f) determination of parameters that GA uses (Michalewicz, 1992).

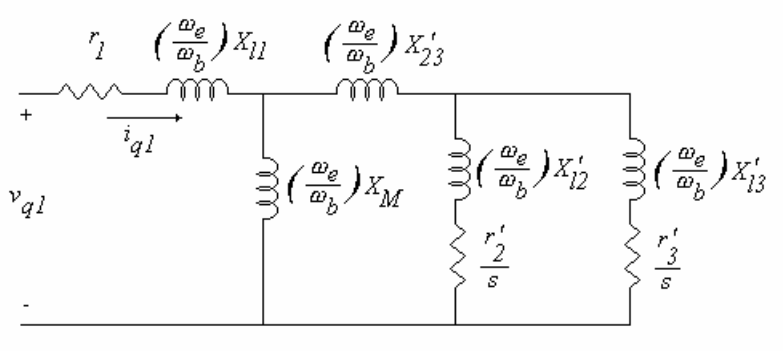

Figure 2. Equivalent circuit of double-cage induction machine

The GA approach relies on the solution of the equations from the equivalent circuit of the DCIM. The nonlinear equations from the equivalent circuit of the machine are constructed such that they form a fitness function that the GA evaluates. A similar approach was proposed by (Nangsue et al, 1999) for a deep bar induction machine.

The input power factor at full-load, electromagnetic torque developed by the machine at the full-load, break-down torque, starting torque and no-load impedance are used in fitness function of genetic algorithm. Hence, the following equations can be written as follows

$$F_1 = 100\left(\frac{3V_{th}^2 r_{e0}}{T_{fl} w_s s_{fl}\left[(r_{th}+\frac{r_{eo}}{s})^2+(x_{th}+x_{run0})^2\right]}-1\right) \tag{6}$$

$$F_2 = 100\left(\frac{3V_{th}^2 r_{e2}}{T_{bd} w_s s_{bd}\left[(r_{th}+\frac{r_{e2}}{s})^2+(x_{th}+x_{run2})^2\right]}-1\right) \tag{7}$$

$$F_3 = 100\left(\frac{3V_{th}^2 r_{e1}}{T_{lr} w_s\left[(r_{th}+\frac{r_{e1}}{s})^2+(x_{th}+x_{run1})^2\right]}-1\right) \tag{8}$$

r_{e0}, r_{e1}, r_{e2} are the full-load, locked-rotor, and breakdown resistances respectively. Similarly, $x_{run0}, x_{run1}, x_{run2}$ are the rotor reactances at full-load, locked-rotor, and breakdown, respectively. Another equation for the full-load power factor equation is written as

$$F_4 = 100\left(\frac{\cos\left(\tan^{-1}\left[\frac{x_{fl}}{r_{fl}}\right]\right)}{pf}-1\right) \tag{9}$$

where pf is the full-load power factor. r_{fl} and x_{fl} are the equivalent circuit resistance and reactance at full-load. Finally, the equation for no-load impedance of the machine is written as

$$F_5 = 100\left(\frac{\sqrt{r_1^2+(x_1+x_m)^2}}{Z_{nl}}-1\right) \tag{10}$$

where Z_{nl} is the no-load impedance. Hence, the fitness function for the genetic algorithm is constructed by combining the equations (6)-(10) and defined as below

$$F = \frac{100}{100 + |F_1| + |F_2| + |F_3| + |F_4| + |F_5|} \tag{11}$$

The fitness function given in equation (11) is evaluated by GA iteratively and the optimum values of the equivalent circuit parameters can be obtained.

2.4 Machine Parameters

The test machine is a 3-phase, Y-connected, squirrel cage, 50 Hz, 4-pole, 380 V, 2.5 kW DCIM. The no-load, locked- rotor, break-down and full-load tests have been performed on the machine while it is Y connected. Friction and windage losses of the machine have been measured to be 40W during the no-load test by gradually decreasing the stator voltage level. The inertia of the induction motor is J=0.02002 kg.m^2 received from the manufacturer. The stator resistance per phase is measured as 3 ohms. The ratio of the resistance of the starting and running cage is also obtained to be $r_3^{'} / r_2^{'} = 0.75$ from the cross sectional areas of bottom and top slots of the rotor structure provided by the manufacturer. This ratio reduces the number of unknown variables estimated in the genetic algorithm. The fitness function given in equation (11) is evaluated by a GA program with the parameters P=100 (population size), N=10000 (generation number), p_c=0.8 (crossover rate), p_m=0.2 (mutation rate). For the given number of iterations, the predicted machine parameters as a result of the GA are obtained and results are given in Table 1

Table 1. The DCIM parameters obtained from GA

r_1	$r_2^{'}$	$r_3^{'}$	x_1	$x_2^{'}$	$x_3^{'}$	$x_{23}^{'}$	$x_m^{'}$
3.0 Ω	5.05 Ω	3.77 Ω	7.51 Ω	0.22 Ω	9.38 Ω	1.39 Ω	169.4 Ω

2.5 Simulation and Experimental Results

The equivalent circuit parameters of the DCIM, which are obtained by GA, have been verified by computer simulations and experimental tests. Also, the validity of the mathematical models has been verified with these equivalent circuit parameters. Simulations are carried out using FORTRAN programming language. In order to investigate the validity of estimated machine parameters from GA, the free acceleration and load tests are carried out on the machine fed by the supply of 230 volts (line to neutral). During the tests, a separately excited dc generator is used as a load having the torque-speed characteristics given below

$$T_L = K\omega_r + T_{fw(g)} + T_{fw(m)} \tag{12}$$

where $T_{fw(g)}$ = 0.62 Nm and $T_{fw(m)}$ = 0.26 Nm are the friction and windage torque values of the generator and motor respectively. K is equal to 0.025 at light load and 0.074 at normal load, which are obtained from the dc generator parameters and the resistance connected to the terminals of the machine. The moment of inertia of the dc generator is 0.0223 kg.m^2 received from the manufacturer. This value is added to the moment of inertia of the motor ($J_T = 0.042\,kg.m^2$, which is the combined moment of inertia) during the simulation under load. During the load tests, the induction motor was initially loaded to a value of K=0.025 and the load was suddenly changed to a value of K = 0.074 by means of the external resistance switched on the terminals of dc generator. The simulation and experimental results of rotor speed are given in Figure 3. The ripples in the experimental speed waveform are due to the tacho-generator used for speed measurement. Transient response of the machine is mostly estimated via simulation with a speed error about %2.7.

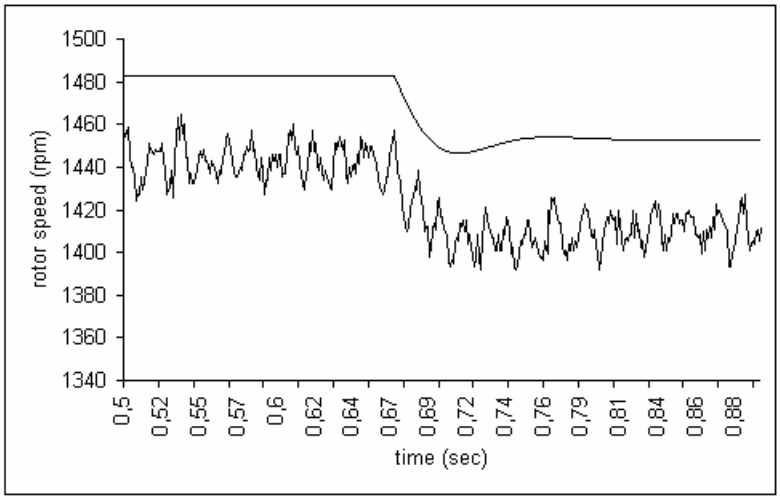

Figure 3. Speed response of the machine during transition from light load to normal load (upper trace-simulation, lower trace-experimental)

In free acceleration test, the shaft of the induction machine is uncoupled from the dc machine and it is started up under 230 volts (phase) directly switched on the stator terminals. The stator phase current is recorded by the data acquisition system. Figure 4 shows the digital simulation and experimental results of phase current for this test taking into account the synchronization between simulation and experimental work at starting instant. It is found that the peak value of starting current deviates from the simulation results and the results of analysis performed on exact equivalent circuit at the steady-state under locked rotor case. The reason is that the leakage reactances are affected from the saturation under heavy starting current. This is verified by applying different level of voltages to the stator as the rotor is blocked The results show that the locked rotor impedance is changing according to the level of stator current while the magnetizing impedance is almost constant and not very much affected by the voltage level during this test.

The torque-slip characteristic of the machine that is obtained from the parameters above is given in Figure 5. It shows that the genetic algorithm properly estimates the machine parameters. If the resistance ratio ($r_3^{'} / r_2^{'} = 0.75$) between the bottom and top slots is not used in the genetic algorithm, the GA still provides an estimation for the rotor resistances fitting the torque slip characteristics but the estimated rotor

resistances deviate from this ratio and it affects the electrical transients as a result of rotor time constant.

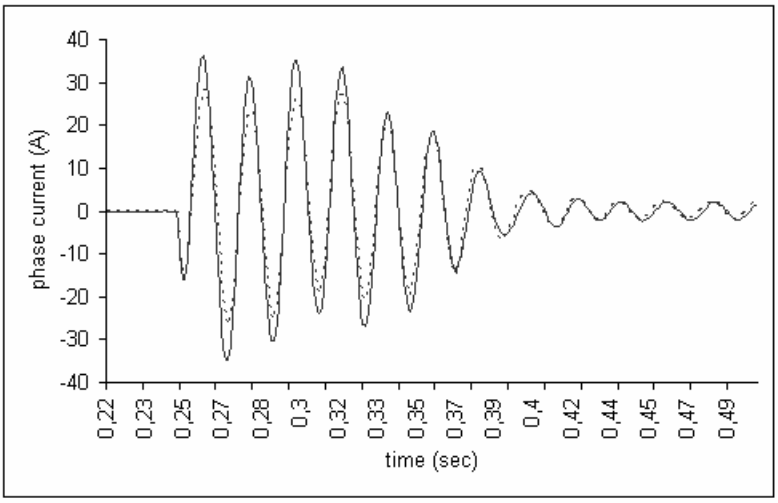

Figure 4. Phase current of the machine during free acceleration test (dotted lines-simulation, continuous lines-experiment)

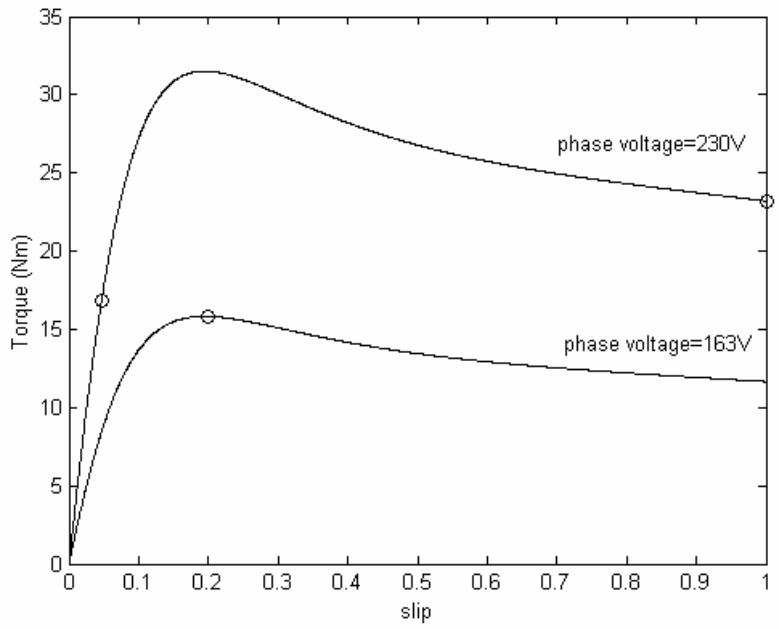

Figure 5. Steady-state torque-slip curves at rated and reduced armature terminal voltage. Continuous lines show the curve obtained from estimated parameters while the dots show measured values.

3. Modeling and Control of Three-Phase PWM Voltage Source Converters

The circuit of the 3-phase PWM ac-dc-ac converter that is used to drive a double-cage induction machine (DCIM) is given in Figure 6. In this scheme, the line-side converter is supplied by balanced three-phase ac voltages and provides a constant dc voltage through the capacitor C. The value of the capacitor should be high enough to minimize the dc ripple voltage and provide energy storage. Series inductors L_s having an internal resistances R_s, are introduced at the ac lines of each phase for filtering of the currents. These inductances are also required for boost operation of the converter.

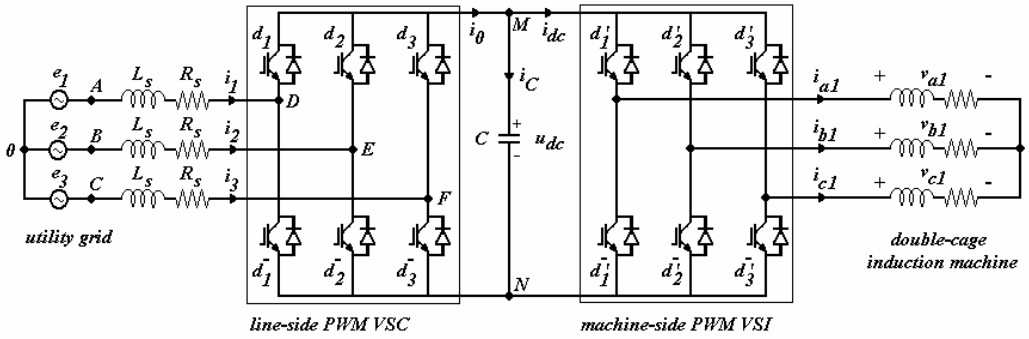

Figure 6. Electrical circuit of 3-phasePWM ac-dc-ac converter

3.1 Modeling and Control of Line-Side PWM Voltage Source Converter

The voltage equations of the line-side converter, which is shown in Figure 6, can be written for each phase. Assuming that the lossless converter is fed from a balanced three-phase system without a neutral connection, the mathematical model of the converter can be derived in convenient compact state-space form as follows (Blasko & Kaura, 1997)

$$L_s \frac{di_k}{dt} + R_s i_k = e_k - (u_{dc} d_k - \frac{u_{dc}}{3} \sum_{k=1}^{3} d_k) \tag{13}$$

$$C\frac{du_{dc}}{dt}=\sum_{k=1}^{3}d_k i_k - i_{dc} \tag{14}$$

where $k=1,2,3$, and R_s, L_s are the resistance and inductance of the inductor connected between converter and ac source. The switching losses of the converter are neglected.

When the current control of the line-side VSC is achieved by a hysteresis current controller, it first generates the command current waveforms and then forces the line currents (i_k) to trace command current waveforms (i_{ck}) within a limited hysteresis band. The appropriate switching waveforms of the switching devices in VSC are obtained from the tracking error of line currents to keep this error in the defined hysteresis band. Since the converter is desired to operate at a specified power factor, the shapes of command currents are simply obtained from the supply voltages, which have the following form:

$$e_k = E_m \sin\left[\omega t-(k-1)\frac{2\pi}{3}\right] \tag{15}$$

Hence, the expression of generated command current waveforms is as follows

$$i_{ck} = I_{cm} \sin\left[\omega t-(k-1)\frac{2\pi}{3}+\theta_{vi}\right] \tag{16}$$

where I_{cm} is magnitude of command currents and θ_{vi} is the desired phase angle. Once the command current waveforms for the converter are obtained, the switching signals are generated according to the following logic:

$$i_{ck}-i_k>\varepsilon_h \;\Rightarrow\; d_k=0, \overline{d}_k=1 \tag{17}$$

$$i_{ck}-i_k<-\varepsilon_h \;\Rightarrow\; d_k=1, \overline{d}_k=0 \tag{18}$$

where $-\varepsilon_h$ and ε_h are the lower and upper limits of the hysteresis band, respectively. If the error in current tracking stays in the hysteresis band, the previous states of the switching signals are preserved.

The generation of command current waveforms is achieved via a closed-loop PI or fuzzy controller. Such a controller regulates the dc link voltage at the desired voltage level and adjusts the magnitude of command currents. Once the required magnitude of ac line currents is calculated, it is formed into command current waveforms of each phase. The hysteresis current controller then forces the ac line currents to track these command current waveforms as described in the previous section. The block scheme of closed-loop hysteresis current controlled line-side voltage source converter is given in Figure 7.

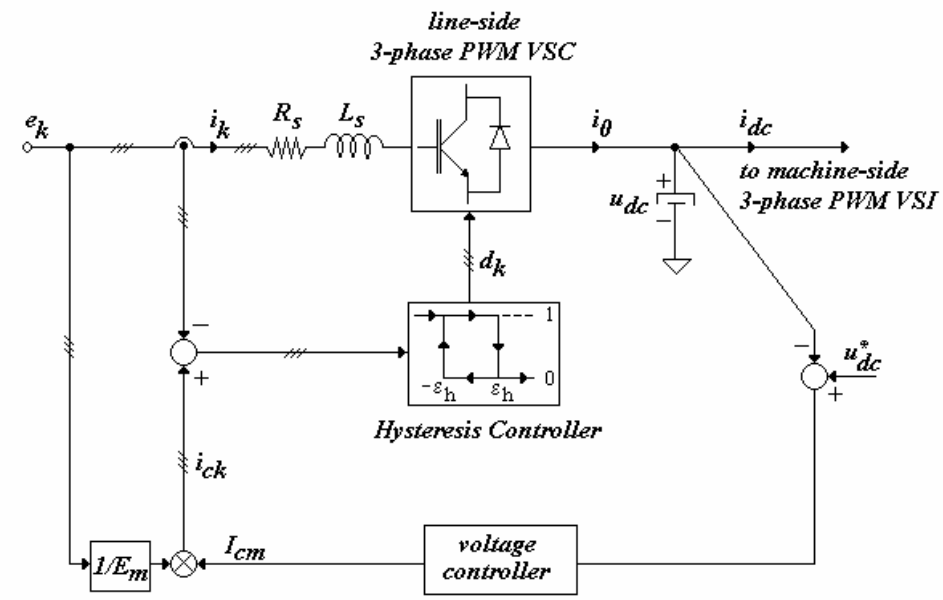

Figure 7. Closed-loop control scheme of 3-phase PWM ac-to-dc converter

3.2 Modeling and Control of Machine-Side PWM Voltage Source Inverter

The voltage source inverters supply variable voltage variable frequency waveforms to ac loads. The ac voltage waveforms are generated through sinusoidal PWM switching pattern, which is simply obtained from sine-triangular wave

comparison. For Y-connected DCIM stator windings, the voltage equations can be obtained by applying the transformation given in equations (19)-(20) to three-phase variables ($i_{abc1}, v_{abc1}, d_k^{'}$) in order to obtain two-phase stationary reference frame model ($\omega = 0$) of the inverter as follows:

$$x_q = \frac{1}{3}(2x_a - x_b - x_c) \tag{19}$$

$$x_d = \frac{1}{\sqrt{3}}(-x_b + x_c) \tag{20}$$

$$v_{q1} = u_{dc} d_q^{'} \tag{21}$$

$$v_{d1} = u_{dc} d_d^{'} \tag{22}$$

where $d_q^{'}, d_d^{'}$ are the transformed inverter switching signals. The dc link current is now expressed in terms of transformed three-phase variables as follows

$$i_{dc} = \frac{3}{2}(i_{qs} d_q^{'} + i_{ds} d_d^{'}) \tag{23}$$

where i_{qs}, i_{ds} are the transformed machine currents.

The closed-loop speed control scheme of DCIM is given in Figure 8. The variable-speed control of DCIM is achieved by adjusting the slip factor by the speed controller, which can be PI or fuzzy controlled. The output of the speed controller forms the desired slip for machine operation (ω_{slip}^{*}). Then the desired slip factor is added to the rotational speed of the DCIM (ω_r) and the command frequency (ω^{*}) signal for PWM VSI is formed. By keeping the V/f ratio constant within zero to rated frequency range, the command voltage signal (V^{*}) required magnitude for ac output voltage is calculated. Above the rated frequency, the V/f ratio is reduced by limiting

the voltage at rated level. This method relies on scalar control by V/f adjustment for induction machine stator voltages. In order to obtain speed feedback signal, a tacho-generator is needed. Since the slip limiter ensures that the machine operates within the defined slip limits, the current drawn by the DCIM is also indirectly limited. Hence, this method does not require an inner current-loop for limiting the machine currents (Dubey, 1989), (Trzynadlowski, 1994).

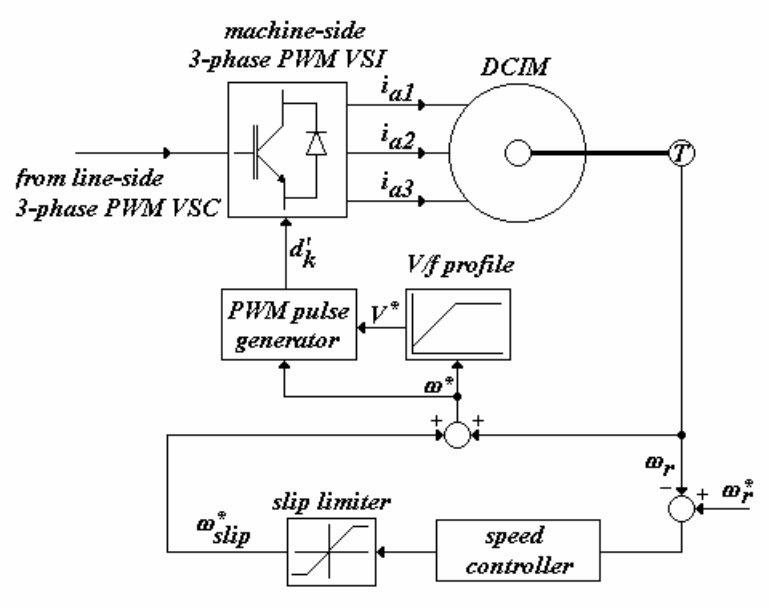

Figure 8. Closed-loop speed control scheme of the DCIM

4. Implementation of PWM Converters in Induction Machine Drive

The proposed drive system has been designed and implemented in laboratory in order to employ it in 2.5 kW wind energy conversion system. The system consists of two back to back PWM converters that are connected between the stator of double-cage induction machine (DCIM) and the utility grid, TMS320F240 digital signal processor (DSP) that performs the control of the drive system, and other electronic circuitry. At the power converter stages, two 6MBP75RA120 FUJI insulated gate bipolar transistor (IGBT) intelligent power modules (IPMs) were used. Each IPM contains 6-pack IGBT, which are rated at 1200V, 75A and provided with internal gate drive and protection circuitry.

Control of the complete system has been performed using a single TMS32F240 16-bit fixed-point digital signal processor (DSP) evaluation module board (EVM). The DSP has TMS320C2XX CPU core with 50ns instruction cycle time, 16K words on-chip flash memory, dual 10-bit on-chip analog to digital converter with multiplexed 16 channels and minimum conversion time of 6.6microseconds, PLL, Watchdog Timer, SCI, SPI, 28 multiplexed multi-functioning I/O ports, and Event Manager with 12 PWM/compare outputs and 3 general purpose timers having the feature of programmable PWM generation with adjustable dead-band, which is especially suitable for digital motor control applications. Also, it has the power drive protection circuitry, which allows the designer to introduce additional protection for power converters in case any fault occurs. The software for controlling the complete system was developed using C compiler provided by Texas Instruments.

4.1 Software Programming

The flowchart of the complete software program is given in Figure 9. The control software for TMS320F240 DSP was developed on Code Composer environment provided by Texas Instruments. Code Composer software is provided with C compiler, assembler, linker, and debugging tools, which are useful in developing programs for Texas DSPs.

4.2 Simulation and Experimental Results

In experiments, a 3-phase, 380V, 50Hz, 4-pole double-cage induction machine was used. In laboratory experiments, the machine was controlled in motoring and generating mode of operation by a Ward-Leonard system, which consists of two back to back connected DC machines. The load torque on the shaft of the DCIM is adjusted via Ward-Leonard system. Hence, bidirectional power flow through the DCIM is achieved. The line-side converter was connected to the ac source at a voltage level of 280V (line to line) and the dc link voltage at the output of the converter was set to 500V. When 280V line-to-line, 3-phase voltage is applied to the input of PWM line-side converter, the dc link capacitance is charged to peak value of

line to line voltage through the anti-parallel diodes of IGBTs. In order to limit charging current of capacitor at startup, a resistance of 470 ohms is connected in series with the capacitor at the output of rectifier and after the capacitor is fully charged, the resistance is bypassed. The switching signals of the line-side converter are applied and the dc link voltage is boosted to its reference value of 500V.

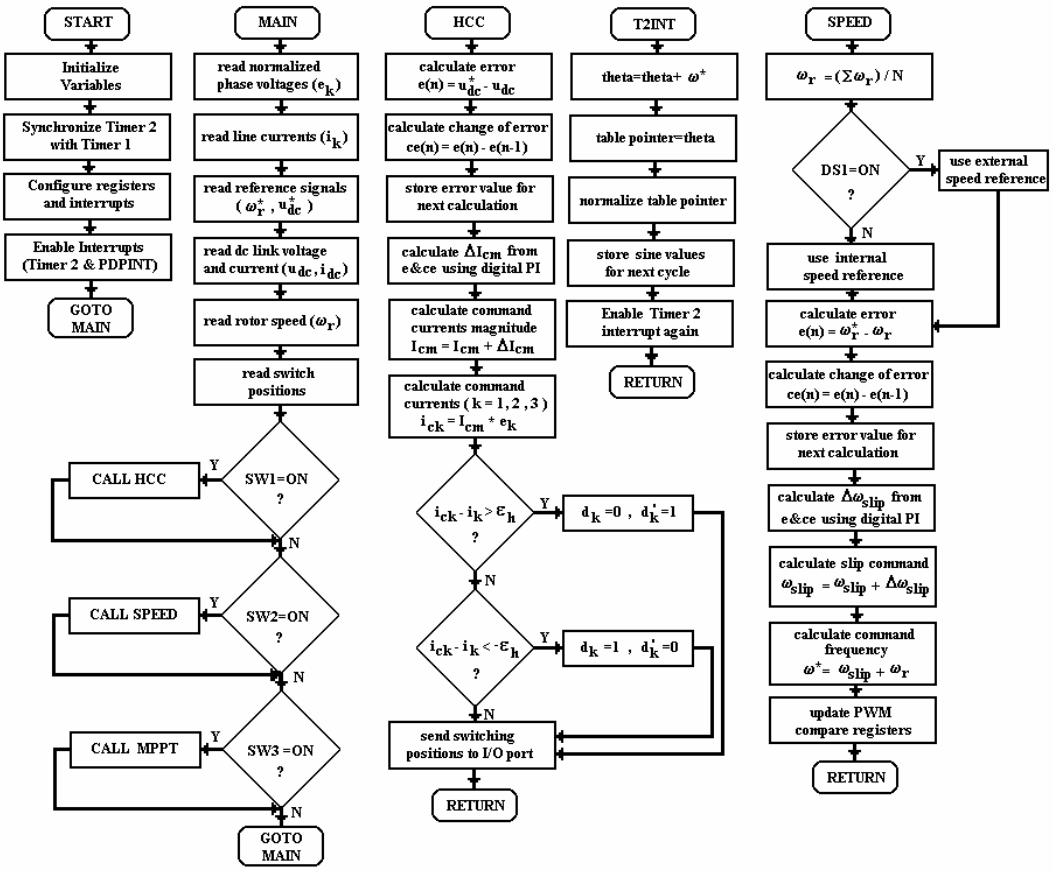

Figure 9. Flow-chart of the developed control software

During the motor operation of the DCIM, the measured value of the shaft torque was 10Nm and the rotor speed is set to 1350rpm. The stator phase current of the DCIM is approximately 6A under this loading condition at steady-state. The line-side converter input voltage and phase current are given in Figure 10. Three-phase, 280V line-to-line voltages have been applied to the converter by means of a variac. The peak value of the line currents is approximately 5A and the average electrical power drawn from the ac line was measured to be nearly 2kW. The simulation results for steady-state phase voltage and current are shown in Figure 11.

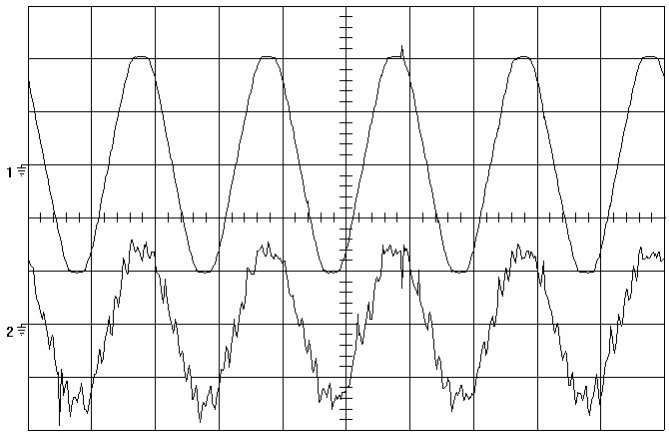

Figure 10. Rectifier operation of the line-side converter observed at motor load test (upper trace: phase voltage-110V/div, lower trace: phase current-4A/div, time/div: 10ms)

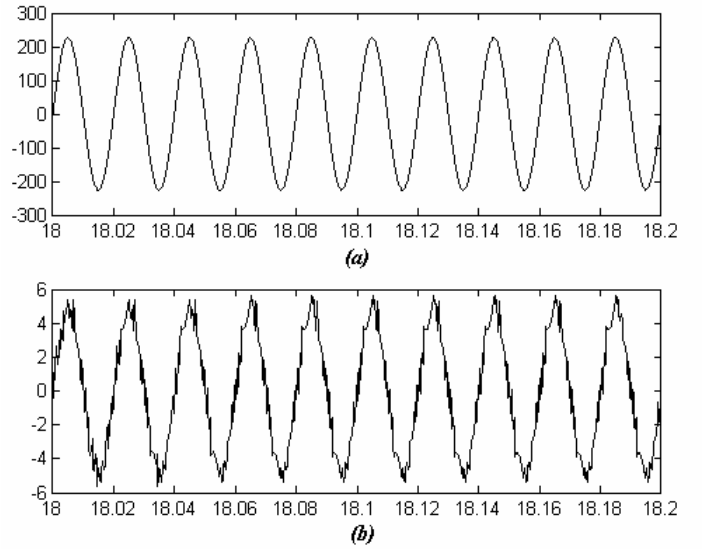

Figure 11. Simulation results for rectifier operation of the line-side converter (a) phase voltage (V) (b) phase current (A)

During the generator operation of the DCIM, the measured value of the shaft torque was -8Nm at 1350 rpm rotor speed, where minus sign indicates the reverse power flow. In Figure 12, the phase voltage and current of the line-side converter are given for generator operation of the DCIM. The power delivered to the ac line was measured to be nearly 1kW. The simulation results of the line voltage and current are given in Figure 13.

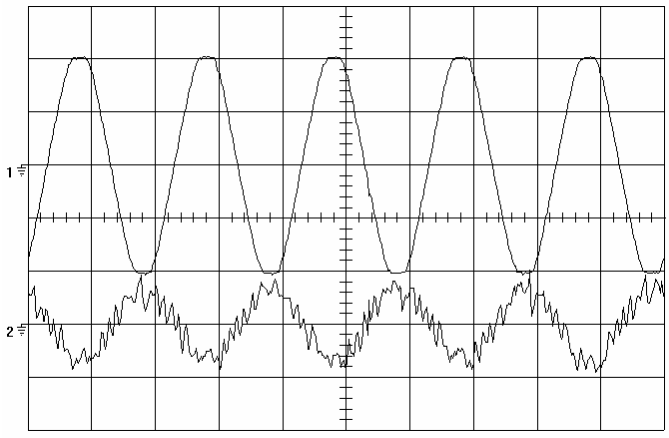

Figure 12. Regenerative operation of the line-side converter observed at generator load test (upper trace: phase voltage-110V/div, phase current-4A/div, time/div: 10ms)

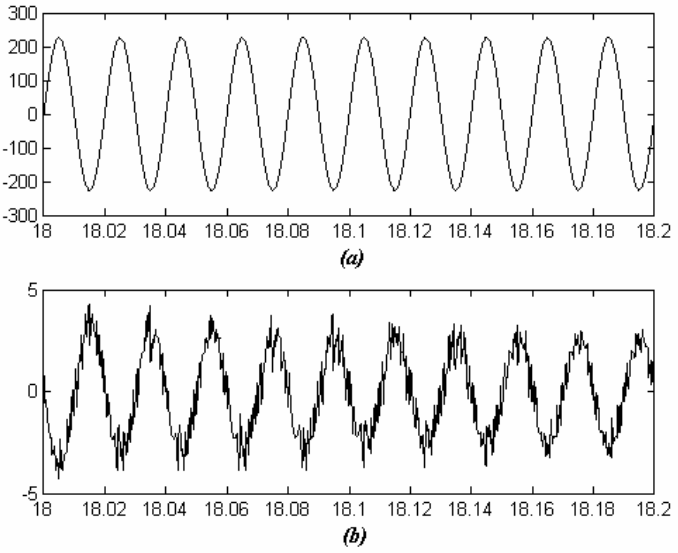

Figure 13. Simulation results for regenerative operation of the line-side converter (a) DCIM phase voltage (V) (b) phase current (A)

In order to extract maximum power from the wind turbine, a search algorithm was implemented in DSP. In MPPT routine, the electrical power is measured via dc link voltage and current, and averaged over 4096 cycles of the program. The speed reference is increased or decreased after each 4096 cycles of the program by a small amount of change (18.75rpm) depending on the changes in electrical power and rotor

speed (Altaş & Sharaf, 1996). Before the algorithm starts, it is assumed the rotor of the DCIM is rotating at a speed (ω_r), determined by the speed reference (ω_r^*). To ensure that operation, first of all, the rotor of the DCIM is rotated by the prime mover. When the rotor speed reaches at a steady-state value, the four quadrant induction machine drive system is started in the procedure described in the previous section. The reference speed value is set to current value of rotational speed and the DCIM is energized via PWM inverter. At this point, the DCIM operates at no-load condition. When the maximum power tracking (MPPT) algorithm is started, the speed reference value is disturbed by a small amount of change ($\Delta\omega_r^*$). The experimental results of dc link voltage and rotor speed are given in Figure 14. Initially, the rotor is running at 820 rpm at no-load driven by the DC motor. When the DCIM is energized via four-quadrant drive, the rotor speed locked at this value. After the MPPT algorithm is started, the drive system searches for the maximum power point. This is obtained at 477 rpm and the developed torque is measured to be 9 Nm.

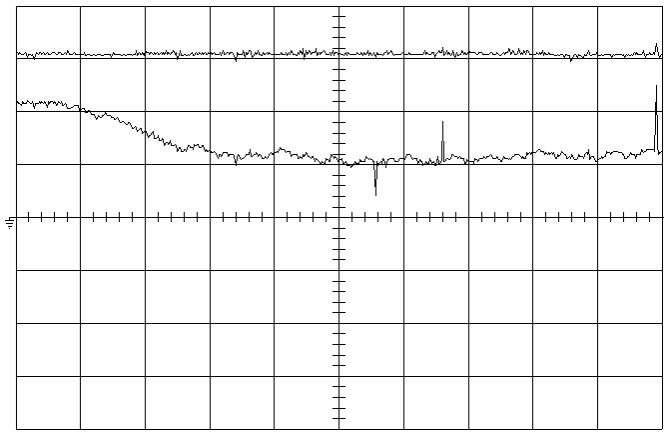

Figure 14. Experimental results during MPPT operation (upper trace: dc link voltage-160V/div, lower trace: rotor speed-375rpm/div, time/div-10s)

5 Experimental Results with Wind Turbine

Experimental works are carried out on the wind turbine designed and implemented. The wind turbine used in the system is a horizontal axis, three-bladed,

fixed pitch angle turbine with a blade length of 2.75m. A free yaw mechanism that consists of a tail vane is used to turn the nacelle to the wind direction such that it is perpendicular to the swept rotor area. The turbine drives the DCIM on the shaft through a gearbox of which speed-up ratio is chosen to be 10. The DCIM is controlled via PWM VSCs to achieve variable-speed operation of the generator.

In experiments, the reference rotor speed of the DCIM is set to a fixed value. For this operating condition of the system, the wind speed, the rms ac line current, the dc link current, and the rotor speed of the DCIM are recorded over a long time range. In Figure 15 the recorded rotor speed of the DCIM over a time range of 545 seconds is shown. During this measurement, rotor reference speed is fixed to 940 rpm and the PI speed controller keeps the actual rotational speed almost stable at the reference value. In normal operating conditions, some small excursions of the actual rotor speed occur due to turbulent wind conditions. Also, a large excursion has been observed during 404-423s due to wind gusts. The line current changes between 2.5A and 0.8A because of shaft power fluctuation. Figure 16 shows the recorded dc link current during measurement. The sign of the dc link current indicates the direction of power flow. The negative value of the dc link current indicates that the power flow is from generator to the grid and inversely from grid to generator for positive values of the dc link current. Especially, during 97-129s, wind condition is quite stable and approximately 1kW power is delivered to the grid. This corresponds to time interval when the wind speed reaches its highest value. The recorded wind speed during this measurement is shown in Figure 17. The system generates constant real power as the wind flows regularly in one direction. Under this condition, the fluctuations in the wind speed are mostly absorbed by the wind turbine due to its high moment of inertia. However, the oscillations in the dc link current, and as a consequence the instantaneous electrical power, can be observed in these long term recordings due to rapidly changing wind direction. The responses of the converters to these rapid changes are satisfactory. The line-side converter quickly responses to the load changes and regulates the dc link voltage at its given reference value. The speed controller also shows a good performance and recovers the rotational speed from the disturbing effects of the wind gusts.

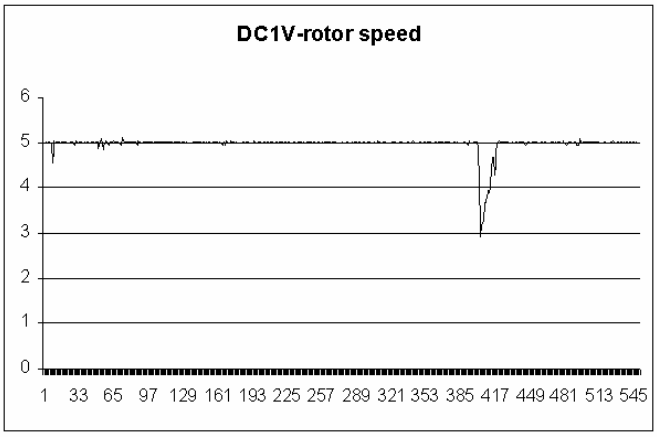

Figure 15. Recorded rotor speed of the DCIM (188 rpm/div)

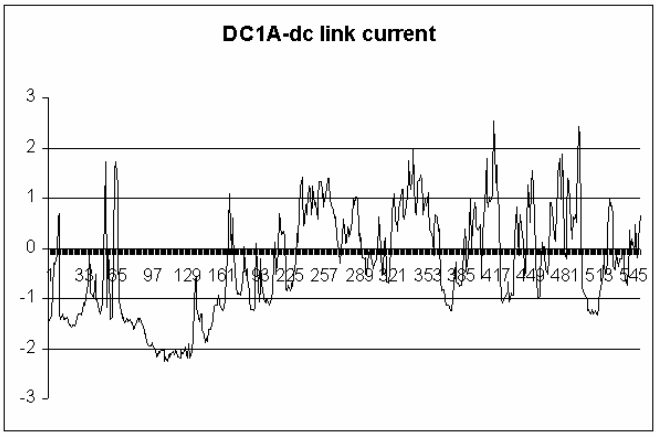

Figure 16. Recorded dc link current at a rotor speed of 940 rpm

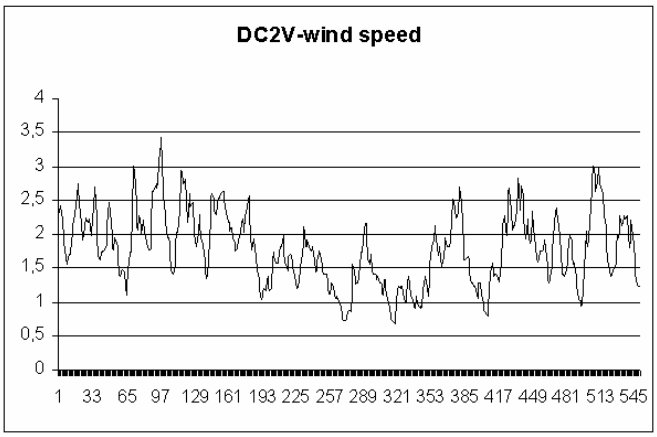

Figure 17. Recorded wind speed at a rotor speed of 940 rpm (3.2m/s/div)

5. Conclusions

The abc/qd and qd/abc models have been obtained for a double-cage induction machine by using the transformations applied for the standard qd/qd model of the machine in reference frame theory. The simulation results during the transient and steady-state operations have been obtained from the models and compared with the test results. The genetic algorithm has been employed for the off-line determination of the motor parameters. This algorithm is sufficiently good for the estimation of these parameters, if the exact equivalent circuit equations in the cost function are properly defined. It is observed that the GA may not converge to a feasible solution if some of those equations are written from exact equivalent circuit and some of them are written from approximate equivalent circuit. Also, the mutual inductance between top and bottom part of the rotor slots, which does not exist in the double-cage induction machine models obtained from universal machine model, is considered in the formulation for the GA. With the equivalent circuit parameters obtained from GA and the derived models of the DCIM, the simulation results depicting the behavior of the machine closely matches to experimental results. However, the measured value of the peak starting current under no-load deviates from the simulation results. The reason for that is the effect of saturation on leakage reactances due to the high starting current, which is not included into the dynamic model of the machine. Also, the breakdown torque used in the GA is measured at the reduced voltage level because the dc machine ratings are not enough to load the induction motor up to breakdown torque under rated voltage. However, the peak of the torque at the rated voltage may not proportionally increase with the square of the voltage due to the saturation in the magnetic circuit.

The mathematical models of the PWM ac-dc-ac converters have been derived and combined with the DCIM model for computer simulations. The modeling of digital PI and fuzzy logic controllers are also included into these models. The system is simulated for motor and generator operation of the DCIM with these two types of controllers. The performance of the fuzzy logic controller due to the variation of the

dc link voltage and rotor speed is found to be slightly better than PI controller with the same controller gains and operating conditions of the system.

The results obtained from simulations are verified by experimental ones carried out on the implemented system in the laboratory. Two back to back DSP based PWM converters are designed to control the power flow in the WECS. The control of the complete system was achieved by one fixed-point DSP. Total execution time of the DSP in one cycle of the program was approximately 250 microseconds, which is enough to control the system. In the implementation of the closed-loop controllers, the PI type is chosen because the execution time of the DSP increases with the application of the FLC due to increasing computational burden. One FLC routine brings an extra computational delay of approximately 200 microseconds and the total execution time of the DSP is almost doubled when a FLC are employed for speed or voltage control instead of PI. As a result, the maximum switching frequency of the line-side converter is reduced since the HCC updates the switching positions over a program cycle. Hence, the current tracking error on the line-side converter increases and this results in poor line current waveforms.

Laboratory tests are carried out for emulating the WECS and to investigate the performance of the implemented drive system. Since the power-speed characteristic of a dc machine is similar to that of wind turbine, the maximum power point tracking routine is also tested on the system in laboratory. This simple search algorithm works well under stable loading conditions and lower moment of inertia of the system.

The performance of the system with a wind turbine is investigated by simulations including the turbine model to the derived converter and machine models. Hence, a complete model of the system is obtained. The implemented drive system is tested with a wind turbine and the electrical quantities are recorded during the operation of the system. Power fluctuations shown in the experimental records are due to turbulent wind conditions. The stability of the converters in the system is satisfactory under randomly varying wind conditions.

References

Ackermann, T., & Söder, L. (2000). Wind Energy Technology and Current Status: a review. Renewable and Sustainable Energy Reviews. 4, 315-374.

Adkins, B., & Harley, R. (1975). The General Theory of Alternating Current Machines: Application to Practical Problems. London: Chapman and Hall.

Akagi, H., Tsukamoto, & Y., Nabae, A. (1990). Analysis and design of an active power filter using quad-series voltage source PWM converter. IEEE Transactions on Industry Applications. 26, no.1, 93-98.

Altas, I.H., & Sharaf, A.M. (1996). A novel on-line MPP search algorithm for PV arrays. IEEE Transactions on Energy Conversion. 11, no.4, 748-754.

Blasko, V., & Kaura, V. (1997). A New Mathematical Model and Control of a Three-Phase AC-DC Voltage Source Converter. IEEE Transactions on Power Electronics. 12, no.1, 116-123.

Buehring, I.K., & Freris, L.L. (1981). Control policies for wind-energy conversion systems. IEE Proceedings. 128, pt. C, no.5, 253-261

Dubey, G.K. (1989). Power Semiconductor Controlled Drives. New York: Prentice-Hall.

Hansen, N.H., Helle, L., Blaabjerg, F., Ritchie, E., Munk-Nielsen, S., Bindner, H., Sorensen, P., & Bak-Jensen, B. (2001). Conceptual Survey of Generators and Power Electronics for Wind Turbines. Denmark: Ris National Laboratory Report.

Kassakian, J.G., Schlecht, M.F., & Verghese, G.C. (1991). Principles of Power Electronics. New York: Addison Wesley Publications.

Khalil, N.A., Tan, O.T., & Baran, I.U. (1982). Reduced Order Models for Double Cage Induction Motors. IEEE Transactions on Power Apparatus and Systems. PAS-101, no. 9, 3135-3140.

Khater, F.M.H. (1996). Power electronics in wind energy conversion systems. Proceedings of Energy Conversion Engineering Conference. 3, 1773-1776.

Krause, P.C., Wasynczuk, O., & Sudhoff, S.D. (1994). Analysis of Electric Machinery. New York: IEEE Press.

Liserre, M. (2001). Innovative control techniques of power converters for industrial automation. Politecnico di Bari, Italy Ph.D. Thesis.

Michalewicz, Z. (1992). Genetic Algorithms + Data Structures = Evolution Programs. New York: Springer.

Nangsue, P., Pillay, P., & Conry, S.E. (1999). Evolutionary Algorithms for Induction Motor Parameter Determination. IEEE Transactions on Energy Conversion. 14, no. 3, 447-453.

Pena, R., Cardenas, R., Blasco, R., Asher, G., & Clare, J. (2001). A cage induction generator using back to back PWM converters for variable speed grid connected wind energy system. Proceedings of IECON 2001. Denver, USA, 2, 1376-1381.

Richards, G. (1988). Reduced Order Model for Single and Double Cage Induction Motors During Startup. IEEE Transactions on Energy Conversion. 3, no. 2, 335-341.

Richards, G., & Sarma, P.R.R. (1994). Reduced Order Models for Induction Motors with Two Rotor Circuits. IEEE Transactions on Energy Conversion. 9, no. 4, 673-678.

Shahalami, S.H., & Saadate, S. (1998). Genetic Algorithm Approaches in the Identification of Squirrel Cage Induction Motor's Parameters. Proceedings of International Conference on Electrical Machines. Istanbul, 908-913.

Simoes, M.G., Bose, B.K., & Spiegel, R.J. (1997). Design and Performance Evaluation of a Fuzzy-Logic Based Variable Speed Wind Generation System. IEEE Transactions on Industry Applications. 33, no. 4, 956-965.

Skvarenina, T.L. (2002). Power Electronics Handbook. New York: CRC Press.

Sürgevil, T., & Akpınar, E. (2003). abc/qd, qd/abc Model of a Double-Cage Induction Machine and Determination of Parameters Using Genetic Algorithm. Journal of Electric Power Components and Systems. 31, no:12, pp: 1115-1131.

Trzynadlowski, A.M. (1994). The Field Orientation Principle in Control of Induction Motors. Boston: Kluwer Academic Publishers.

Walker, J.F., & Jenkins, N. (1997). Wind Energy Technology. Chichester: John Wiley & Sons

WEB_1 (2003). American Wind Energy Association Web Site. Complimentary Resource Library, Wind Power Outlook. http://www.awea.org/pubs/complimentary.html. 15/12/2003.

Zinger, D.S., Muljadi, E. (1997). Annualized Wind Energy Improvement Using Variable-Speeds. IEEE Transactions on Industry Applications. 33, no.6 1444-1447.